

A Molecular Face-on View of the Galactic Centre Region

Tsuyoshi Sawada,^{1,2,3*} Tetsuo Hasegawa,^{2,3} Toshihiro Handa³ and R. J. Cohen⁴

¹*Nobeyama Radio Observatory, 462-2 Nobeyama, Minamimaki, Minamisaku, Nagano 384-1305, Japan*

²*National Astronomical Observatory of Japan, 2-21-1 Osawa, Mitaka, Tokyo 181-8588, Japan*

³*Institute of Astronomy, University of Tokyo, 2-21-1 Osawa, Mitaka, Tokyo 181-0015, Japan*

⁴*Jodrell Bank Observatory, University of Manchester, Macclesfield, Cheshire SK11 9DL*

Accepted 2004 January 12. Received 2003 October 11

ABSTRACT

We present a method to derive positions of molecular clouds along the lines of sight from a quantitative comparison between 2.6 mm CO emission lines and 18 cm OH absorption lines, and apply it to the central kiloparsecs of the Milky Way. With some simple but justifiable assumptions, we derive a face-on distribution of the CO brightness and corresponding radial velocity in the Galactic centre without any help of kinematical models. The derived face-on distribution of the gas is elongated and inclined so that the Galactic-eastern (positive longitude) side is closer to us. The gas distribution is dominated by a barlike central condensation, whose apparent size is 500 × 200 pc. A ridge feature is seen to stretch from one end of the central condensation, though its elongated morphology might be artificial. The velocity field shows clear signs of noncircular motion in the central condensation. The ‘expanding molecular ring’ feature corresponds to the peripheral region surrounding the central condensation with the Galactic-eastern end being closer to us. These characteristics agree with a picture in which the kinematics of the gas in the central kiloparsec of the Galaxy is under a strong influence of a barred potential. The face-on distribution of the *in situ* pressure of the molecular gas is derived from the CO multiline analysis. The derived pressure is found to be highest in the central 100 pc. In this region, the gas is accumulating and is forming stars.

Key words: ISM: molecules – Galaxy: centre – Galaxy: kinematics and dynamics – radio lines: ISM

1 INTRODUCTION

The behavior of molecular gas, in particular its physical conditions and kinematics, in central regions of galaxies is key information to understand the star forming activity which occurs there. The Galactic centre can be observed in much greater detail compared with central regions of other galaxies. However, its inevitable edge-on perspective sometimes complicates the interpretation of the data. In particular, a face-on image of the Galactic centre is very hard to construct, though such an image would be very helpful to understand its kinematics and to make a comparison with central regions of other galaxies. Attempts have been made to construct models of gas kinematics (see, e.g., Liszt & Burton 1980; Binney et al. 1991; Fux 1999). Their models give more or less reasonable interpretation of some aspects of the distribution and motion of the gas, in particular its asymmetric position-velocity appearance and some outstanding features. Kinematical models can be used to

project position-velocity diagrams of molecular/atomic line data into a face-on view (see, e.g., Cohen & Dent 1983; Sofue 1995; Nakanishi & Sofue 2003). This is an indirect method to investigate the spatial distribution of the gas: it would be invaluable if we could derive positions of molecular clouds independent of kinematical assumptions. The molecular content and star forming regions in the Galactic centre are strongly confined in the central a few hundred parsecs: the region is called the central molecular zone (CMZ; Morris & Serabyn 1996). Though the kinematics and face-on distribution of the gas within the CMZ are essential information to study the star forming activity in the Galactic centre, they are complicated and less well understood than the outer region (up to the Galactocentric radius of a few kpc) mainly traced by atomic hydrogen line.

In this paper, we present a method to derive a molecular face-on view of the Galactic centre without any help of kinematical models. In § 2 we describe the basic methodology. Using that, we draw a face-on distribution of the molecular gas from existing data and discuss the resultant face-on

* E-mail: sawada@nro.nao.ac.jp

view in § 3. Physical conditions of the gas and the validity of parameters used in the model are also discussed.

2 THE METHOD

The essence of our method lies in comparing emission and absorption spectra toward the Galactic centre. We compare the CO 2.6 mm emission with the OH 18 cm absorption. Because the Galactic centre region itself is an intense diffuse 18 cm continuum source, strong OH absorption arises preferentially from the gas that lies in front of the continuum regions, rather than gas that lies behind them. On the other hand, the CO emission samples the gas both in front and back of the continuum sources equally. Thus the OH/CO ratio carries information on the position of the gas along the line of sight relative to the continuum sources. In the following, we devise a method to estimate the position quantitatively by introducing some simple assumptions.

2.1 Qualitative inspection on molecular gas distribution

We used the Columbia-U. Chile ^{12}CO $J = 1 - 0$ data (Bitran et al. 1997) and a large-scale absorption survey of the OH main lines (1665 MHz and 1667 MHz) made by Boyce & Cohen (1994). Both data were binned over successive 5 km s^{-1} velocity ranges. The CO data, for which the original resolution and grid spacing are respectively 9 arcmin and 7.5 arcmin, were smoothed to 10-arcmin resolution and resampled with a 12-arcmin grid to match the OH data. Hereafter we mainly used the 1667 MHz line for the OH absorption. However, because of the large velocity spread of the molecular clouds in the Galactic centre, the positive-velocity end of the 1667 MHz line blends together with the negative-velocity end of the 1665 MHz line. Thus we replaced the $v_{\text{LSR}} > 100 \text{ km s}^{-1}$ part of the 1667 MHz line with the 1665 MHz data scaled by 1.37, which is the mean ratio of the absorption depth between the two lines in the velocity range $25 \leq v_{\text{LSR}} \leq 100 \text{ km s}^{-1}$.

Figure 1 shows the processed spectra of the OH absorption and the CO emission at $(\ell, b) = (-0^\circ.2, 0^\circ.0)$. This figure demonstrates that the OH/CO ratio varies significantly as a function of the radial velocity, v_{LSR} . For example, we may draw attention to the velocity components near $v_{\text{LSR}} \simeq -130 \text{ km s}^{-1}$ and $v_{\text{LSR}} \simeq 160 \text{ km s}^{-1}$ (shadowed in Fig. 1), both of which belong to the so-called ‘expanding molecular ring’ (EMR; Kaifu, Kato & Iguchi 1972; Scoville 1972). The CO intensities at these components are almost the same. This suggests that the amounts of molecular gas are similar in each component. On the other hand, the OH absorption depths are strikingly different. The negative-velocity component shows deep absorption, while there is no distinct absorption around the positive-velocity component. We immediately deduce from this fact that the negative-velocity component is located in front of strong continuum source surrounding the Galactic centre, while the positive-velocity component is behind it. This logic led Kaifu et al. (1972) to conclude that this feature is expanding away from the Galactic centre.

Figure 2 shows the longitude-velocity (ℓ - v) diagram of the ratio between the OH apparent opacity ($\tau_{\text{app}} \equiv$

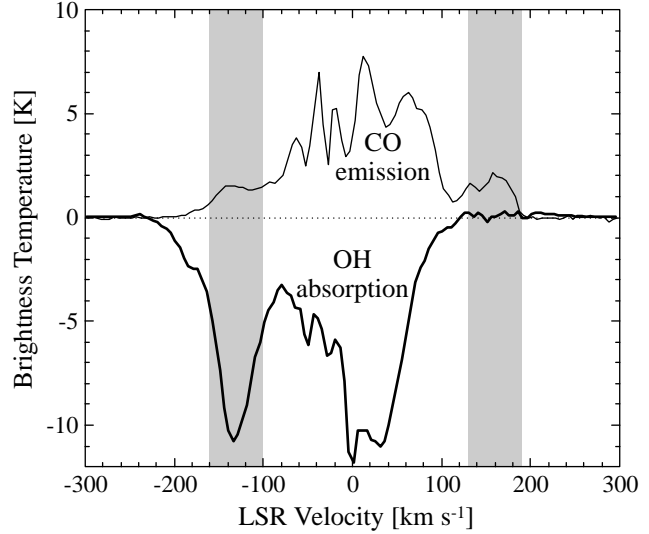


Figure 1. Sample spectra of CO emission (thin line) and OH absorption (thick line) at $(\ell, b) = (-0^\circ.2, 0^\circ.0)$. Shadowed velocity components demonstrate the difference of cloud position along the line of sight (see text).

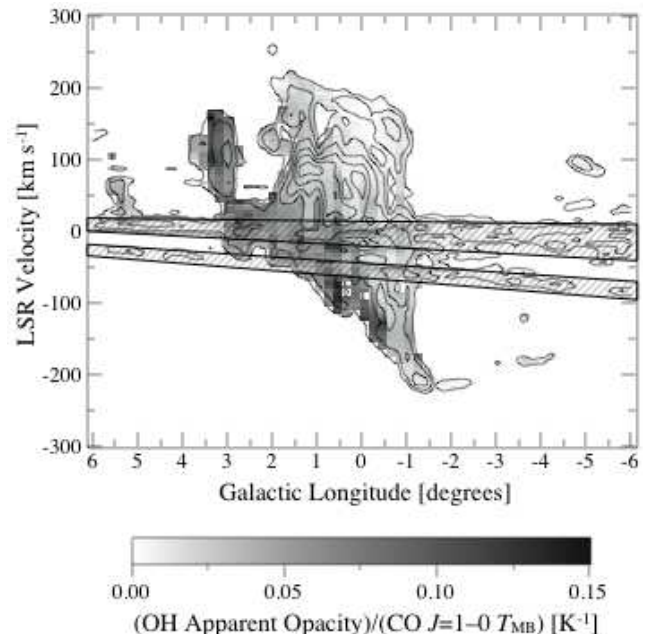


Figure 2. The ratio between the OH apparent opacity and the CO $J = 1 - 0$ intensity at $b = 0^\circ.0$. Contours are $T_{\text{MB}}(\text{CO}) = 1, 2, 4, 7, 10$, and 14 [K] . The ratio is shown in the region where $T_{\text{MB}}(\text{CO})$ exceeds 1 [K] . Hatched velocity ranges were excluded from the analysis because of contamination by clouds well outside the Galactic centre region.

$T_{\text{abs}}/T_{\text{cont}}$; where T_{abs} and T_{cont} are line absorption and continuum antenna temperatures, respectively) and the CO $J = 1 - 0$ line intensity. The ratio has a clear trend; it is smaller in $\ell < 0^\circ$ and $v_{\text{LSR}} > 0 \text{ km s}^{-1}$, while it is larger in $\ell > 0^\circ$ and $v_{\text{LSR}} < 0 \text{ km s}^{-1}$ and in the feature with extremely large velocity width at $\ell \simeq 3^\circ$, which is called Bania’s Clump 2 (Bania 1977). The ratio in the velocity

range $-60 \text{ km s}^{-1} \lesssim v_{\text{LSR}} \lesssim 10 \text{ km s}^{-1}$ is affected by the foreground gas in the Galactic disc and does not show the intrinsic value of the Galactic centre. Thus the hatched velocity ranges in Fig. 2 are excluded from the following analysis.

2.2 Deriving distances to clouds

Based upon the logic shown in the previous section, we extend it to quantitative estimation of molecular gas distribution. In order to determine the distances to molecular clouds quantitatively, we adopt the following four assumptions:

- (1) At a given ℓ , emission observed at each velocity bin comes from a single position along the line of sight.
- (2) The CO line intensity T_{CO} at a given velocity is proportional to the amount of molecular gas in unit velocity width; and the OH opacity τ_{OH} (not the ‘apparent’ one but the real one) at a given velocity is also proportional to the amount of molecular gas in unit velocity width. Consequently, $\tau_{\text{OH}} = Z T_{\text{CO}}$ where Z is a constant.
- (3) The excitation temperature of OH [$T_{\text{ex}}(\text{OH})$] is uniform.
- (4) The 18 cm continuum emission is optically thin and arises from a distributed volume emissivity, $j(r)$ [r is the Galactocentric radius], that is axisymmetric about the Galactic centre as modelled in § 2.3.

Now Z and $T_{\text{ex}}(\text{OH})$ are unknown parameters. How to determine them is described in § 2.4; validity of them and the assumption (1) are discussed in § 3.3.

When a cloud whose OH opacity is τ_{OH} is located at $s = s_0$ (s is the position along the line of sight), the cloud absorbs the continuum intensity behind it, i.e., the continuum emissivity integrated along the line of sight behind the cloud, $\int_{-\infty}^{s_0} j(r) ds$ using the assumption of optically thin continuum emission. The absorption depth is written as $f[1 - \exp(-\tau_{\text{OH}})][\int_{-\infty}^{s_0} j(r) ds - T_{\text{ex}}(\text{OH})]$ where f is the beam filling factor of OH absorbing gas. The total continuum intensity observed by us is $\int_{-\infty}^{s_0} j(r) ds$, and the apparent opacity τ_{app} of the cloud is expressed as

$$\tau_{\text{app}} = \frac{f[1 - \exp(-\tau_{\text{OH}})][\int_{-\infty}^{s_0} j(r) ds - T_{\text{ex}}(\text{OH})]}{\int_{-\infty}^{s_0} j(r) ds}. \quad (1)$$

Since τ_{app} and T_{CO} (and thus $\tau_{\text{OH}} = Z T_{\text{CO}}$) are known through the observations, we can obtain the value of $\int_{-\infty}^{s_0} j(r) ds$ if we know f , Z , and $T_{\text{ex}}(\text{OH})$. Then s_0 is derived from the value of $\int_{-\infty}^{s_0} j(r) ds$ using a distribution model of $j(r)$.

2.3 Modelling the distribution of continuum emissivity

We assume that the 18 cm continuum emissivity $j(r)$ around the Galactic centre is described as a sum of several axisymmetric Gaussians:

$$j(r) = \sum_{i=1}^N \frac{a_i}{\sqrt{2\pi}\sigma_i} \exp\left(-\frac{r^2}{2\sigma_i^2}\right) \quad (2)$$

$$\simeq \sum_{i=1}^N \frac{a_i}{\sqrt{2\pi}\sigma_i} \exp\left(-\frac{\ell^2 + s^2}{2\sigma_i^2}\right). \quad (3)$$

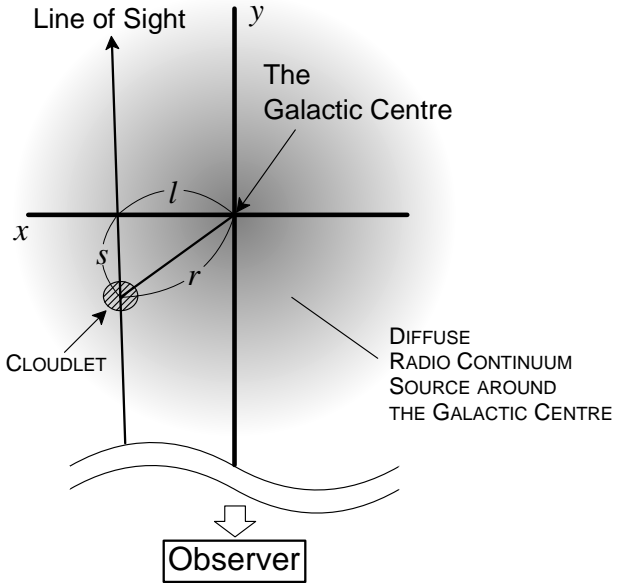


Figure 3. The schematic relation of geometrical parameters in the face-on view of the Galactic centre region.

Figure 3 shows the schematic relation of geometrical parameters. The Galactic longitude ℓ is in degrees. Here r , s , and σ_i are in units of projected distance corresponding to 1° at the distance to the Galactic centre: i.e., 150 pc at 8.5 kpc. The observed longitudinal distribution of the continuum brightness $T_{\text{cont}}(\ell)$ can be written as

$$T_{\text{cont}}(\ell) = \int_{-\infty}^{s_0} j(r) ds. \quad (4)$$

Since the continuum emissivity beyond the solar circle should be negligible compared with that in the centre, $\int_{-\infty}^{s_0} j(r) ds$ can be replaced with $\int_{-\infty}^{\infty} j(r) ds$. Thus

$$T_{\text{cont}}(\ell) \simeq \int_{-\infty}^{\infty} \left[\sum_{i=1}^N \frac{a_i}{\sqrt{2\pi}\sigma_i} \exp\left(-\frac{\ell^2 + s^2}{2\sigma_i^2}\right) \right] ds \quad (5)$$

$$= \sum_{i=1}^N a_i \exp\left(-\frac{\ell^2}{2\sigma_i^2}\right). \quad (6)$$

Now a_i and σ_i can be drawn so that the Eq. (6) reproduces the observed longitudinal distribution of the continuum brightness. It is found that observed continuum distribution is well fitted by up to three components ($N = 3$). For $b = 0^\circ 0$, we obtain $a_1 = 98.3$, $a_2 = 34.0$, $a_3 = 11.4$; $\sigma_1 = 0.120$, $\sigma_2 = 0.677$, $\sigma_3 = 7.18$. Parameters a_i are in Kelvins, and σ_i are in degrees. Figure 4 shows the result of our fit. The model reproduces the observed data quite well.

Since σ_1 , σ_2 are small enough ($\lesssim 100$ pc) and a_1 , a_2 are large, the continuum distribution due to the first ($i = 1$) and the second ($i = 2$) components is well defined. In some galaxies seen in nearly face-on perspective, such as M83 (Ondrechen 1985) and IC 342 (Crosthwaite, Turner & Ho 2000), $\lambda \simeq 20$ cm continuum emission in the central kiloparsec consists of strong central source and extended emission seen in resolutions of hundreds of parsecs. For such

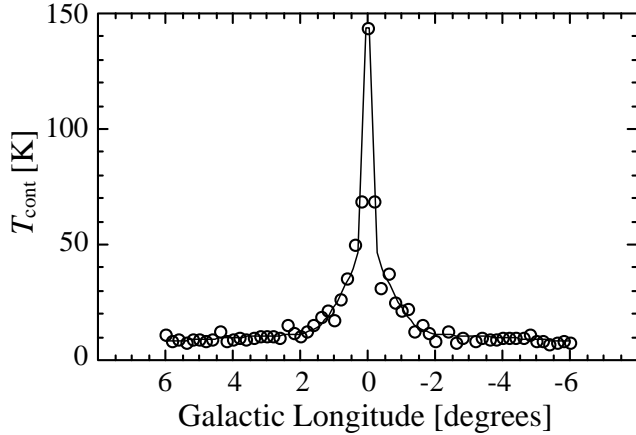


Figure 4. Longitudinal distribution of the 18 cm continuum in units of antenna temperature at $b = 0.0$ by Boyce & Cohen (1994) (open circles) and a fit by 3 Gaussians (solid line). The fitting function is $T_{\text{cont}} = \sum_{i=1}^3 a_i \exp(-\ell^2/(2\sigma_i^2))$ where $a_1 = 98.3 \text{ [K]}$, $a_2 = 34.0 \text{ [K]}$, $a_3 = 11.4 \text{ [K]}$; $\sigma_1 = 0^\circ 120$, $\sigma_2 = 0^\circ 677$, $\sigma_3 = 7^\circ 18$.

continuum distribution, axisymmetric emissivity distribution is a good approximation in the first order. On the other hand, there are galaxies whose central $\lambda \simeq 20$ cm emission is dominated by ring structure, such as NGC 1097 (Hummel, van der Hulst & Keel 1987) and NGC 1365 (Sandqvist, Jörsäter & Lindblad 1995). This is not the case for the Milky Way Galaxy because the 18 cm continuum brightness in the Galactic centre, our edge-on view, has an intense central peak with a monotonic decrease away from the centre (see Fig. 4). The fact that the central peak, which should originate in the Sgr A region, is seen through the foreground medium supports our assumption that the 18 cm continuum is optically thin.

On the other hand, because of large σ_3 and small a_3 , the third ($i = 3$) component should suffer from possible non-axisymmetric distribution on the largest scale and/or individual sources; furthermore, small dT_{cont}/ds causes large errors in the derived positions of clouds. Therefore, in longitudes where the contribution from the first and the second components is negligible (i.e., $|\ell| \gtrsim 1^\circ 5$), the positions of clouds obtained using this model are rather uncertain.

2.4 Choice of the Z and $T_{\text{ex(OH)}}$ values

Following the procedure, we can draw a face-on (x - y) distribution of the molecular gas by putting each data point of the ℓ - v diagram (Fig. 2) on to the x - y plane with a projection of $(\ell, s) \rightarrow (x, y)$. However, f , Z , and $T_{\text{ex(OH)}}$ are still unknown. Here we assume $f = 1$: the validity of this assumption is discussed in § 3.3.1. There is no bottom-up scheme to determine Z and $T_{\text{ex(OH)}}$. To determine Z and $T_{\text{ex(OH)}}$, we employ a trial-and-error scheme, making face-on maps at $b = +0^\circ 4, +0^\circ 2, 0^\circ 0, -0^\circ 2$, and $-0^\circ 4$ with various values of Z and $T_{\text{ex(OH)}}$. The data used, i.e., the OH/CO ℓ - v diagrams and the continuum distribution, are shown in Figures

5 and 6. Trials have been done for $Z = 0.04$ to $0.70 \text{ [K}^{-1}]$ and $T_{\text{ex(OH)}} = 0$ to 10 [K] ¹.

We have chosen an appropriate set of $(Z, T_{\text{ex(OH)}})$ so that the following three conditions are satisfied:

- (1) The resultant face-on distribution of the CO brightness is not too asymmetric between the near and far sides with respect to the centre,
- (2) The features extending above and below the Galactic plane are placed in similar face-on positions at different latitudes, and
- (3) Most of the CO emission has a solution for the position s_0 .

In order to check the condition (1), the CO emission within $|\ell| \leq 1^\circ$ is treated. The percentage of the CO emission located in the near side ($s_0 > 0$) is displayed in Figure 7a. The central molecular emission has a well-known asymmetry with respect to $\ell = 0^\circ$: Bally et al. (1988) mentioned that about three-fourths of molecular (¹³CO and CS) emission comes from positive longitudes. Therefore asymmetry to a similar degree along the line of sight is acceptable. Sets of large Z and small $T_{\text{ex(OH)}}$ are rejected since they would put most of the emission on the far side.

A cloud complex around $(\ell, v_{\text{LSR}}) \simeq (1^\circ 3, +100 \text{ km s}^{-1})$ [hereafter the '1.3 region'] is chosen to check the condition (2). At first we have derived the centres of emission along the lines of sight in $b = 0^\circ 0, \pm 0^\circ 2, \pm 0^\circ 4$. Then the standard deviation of the centres is calculated: Figure 7b shows the results. The standard deviation becomes small when we adopt $Z \gtrsim 0.10 \text{ [K}^{-1}]$ and $T_{\text{ex(OH)}} \simeq 4 \text{ [K]}$. The gas at high latitudes goes farther with respect to that at $b = 0^\circ 0$ if we adopted smaller values for $T_{\text{ex(OH)}}$; the reverse is also true.

For the condition (3), we deal with Clump 2. Because of its large OH/CO ratio, Clump 2 is apt to have no solution; i.e., the large absorption depth cannot be reproduced even if the cloud is located just in front of us. Figure 7c shows the percentage of the CO emission which can be placed within $-3750 < s_0 < 3750 \text{ pc}$ for the used sets of $(Z, T_{\text{ex(OH)}})$. If we use small Z or large $T_{\text{ex(OH)}}$, significant emission is lost.

By combining these conditions, we have chosen $Z = 0.15 \pm 0.03 \text{ [K}^{-1}]$ and $T_{\text{ex(OH)}} = 4 \pm 1 \text{ [K]}$. As noted in § 2.3, the derived distances to the clouds are uncertain in $|\ell| \gtrsim 1^\circ 5$. Thus the constraint on the parameters given by condition (3) using Clump 2 ($\ell \simeq 3^\circ$) is weaker than those given by conditions (1) and (2). However, parameter space allowed by condition (2) is involved in that given by condition (3). Thus we can obtain $(Z, T_{\text{ex(OH)}}) = (0.15 \pm 0.03 \text{ [K}^{-1}], 4 \pm 1 \text{ [K]})$ using the conditions (1) and (2) alone; condition (3) is then automatically satisfied.

3 RESULTS AND DISCUSSION

3.1 Distribution and kinematics of the gas

3.1.1 Overall structure

Figure 8 shows the resultant molecular face-on view of the Galactic centre region at $b = 0^\circ 0$ seen from the direction of the north Galactic pole. The CO brightness of each pixel

¹ $T_{\text{ex(OH)}}$ is measured as an excess over the cosmic microwave background (CMB).

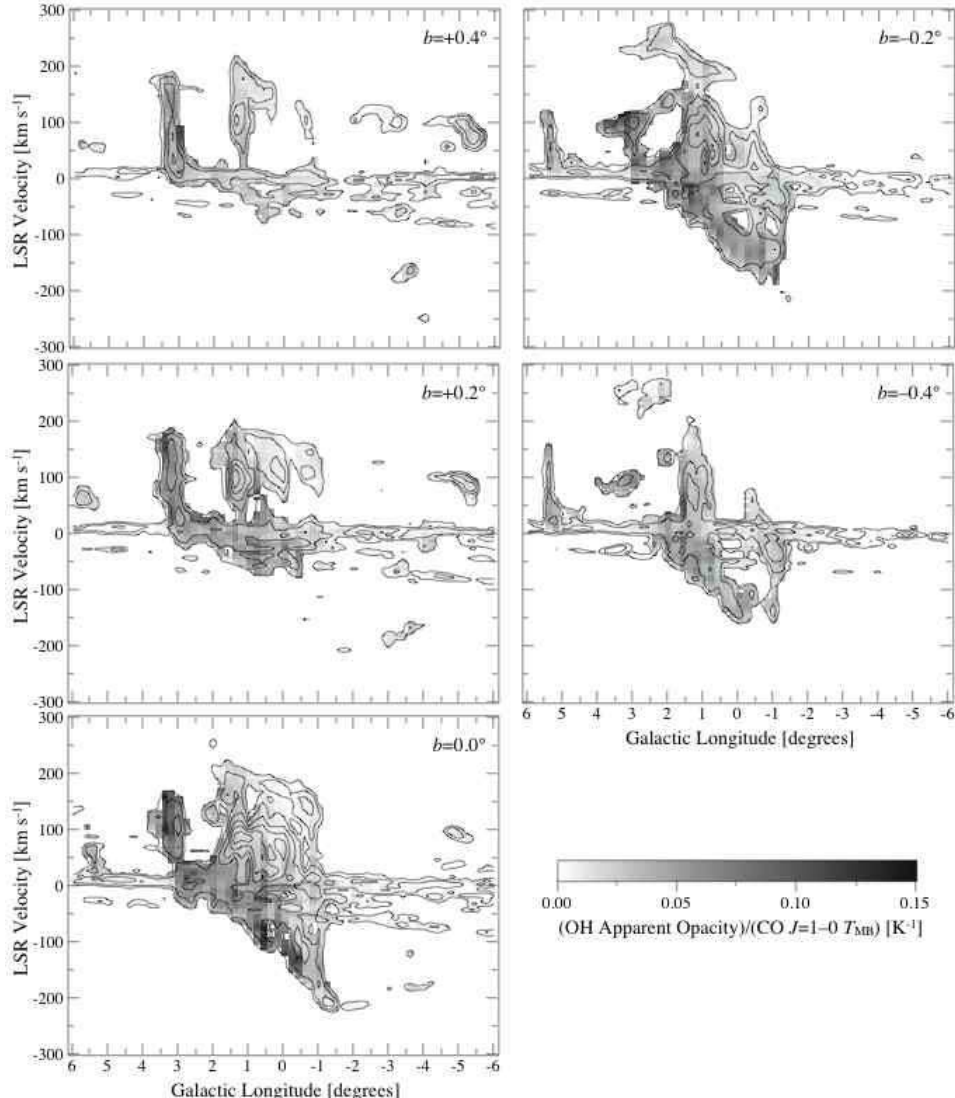


Figure 5. Longitude-velocity distribution of the OH/CO ratio, shown in the same way as Fig. 2.

in Fig. 2 is projected on to the x - y plane and smoothed by $\sigma = 20$ pc Gaussian. Figures 8a and 8b show the distributions of CO brightness and corresponding radial velocity, respectively. Dashed lines in the Figure indicate $\ell = \pm 1.5^\circ$: as mentioned in § 2.3, the obtained face-on maps are less reliable outside them.

The resultant CO distribution mainly consists of a central condensation (corresponding to the CMZ) and a thin ridge feature at $(x, y) \simeq (400 \text{ pc}, -1000 \text{ pc})$ that stretches almost along the line of sight from the Galactic-eastern (positive x in Fig. 8) end of the central condensation. As seen in Fig. 2, high OH/CO ratio is more widespread in the positive longitudes. This comes about because the face-on CO distribution is inclined so that the gas in the positive x (corresponding to positive ℓ) lies closer to us, as qualitatively suggested by Cohen & Few (1976). It has long been argued that the Milky Way is a barred galaxy. Recent studies agree with a picture in which the Galactic-eastern (positive longitude) end of the bar is closer to us (see, e.g., Morris & Serabyn

1996; Gerhard 1999, and references therein). Our face-on map shows, as a whole, the same trend as this picture.

Some barred galaxies, such as NGC 1097 (Ondrechen & van der Hulst 1983; Hummel et al. 1987) and M83 (Ondrechen 1985), show $\lambda \simeq 20$ cm continuum enhancements in their bars; in particular, in the dust lanes. If the Milky Way is barred and the 18 cm continuum emissivity is elongated along its bar like these galaxies, then the actual distribution of molecular gas would be *more* inclined than that obtained here. Therefore the trend of inclination is very certain.

3.1.2 Central condensation

The central condensation dominates the CO emission in the Galactic centre region. It is elongated: its apparent size is approximately 500×200 pc, and should be compared with ‘twin peaks’ in central regions of barred galaxies (Kenney et al. 1992). The minor axis length of the condensation might be smaller since the face-on map involves positional errors along

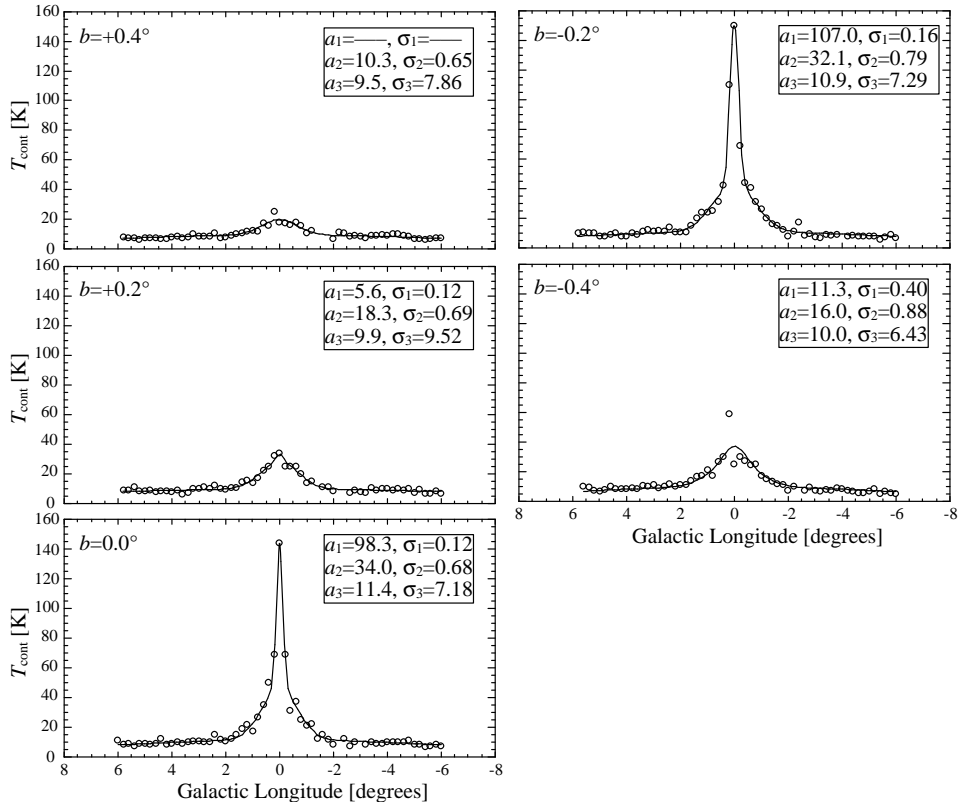


Figure 6. Longitudinal distribution of the 18 cm continuum brightness and model fits shown in the same way as Fig. 4. The fit parameters a_i and σ_i ($i = 1, 2, 3$) are in Kelvins and degrees, respectively.

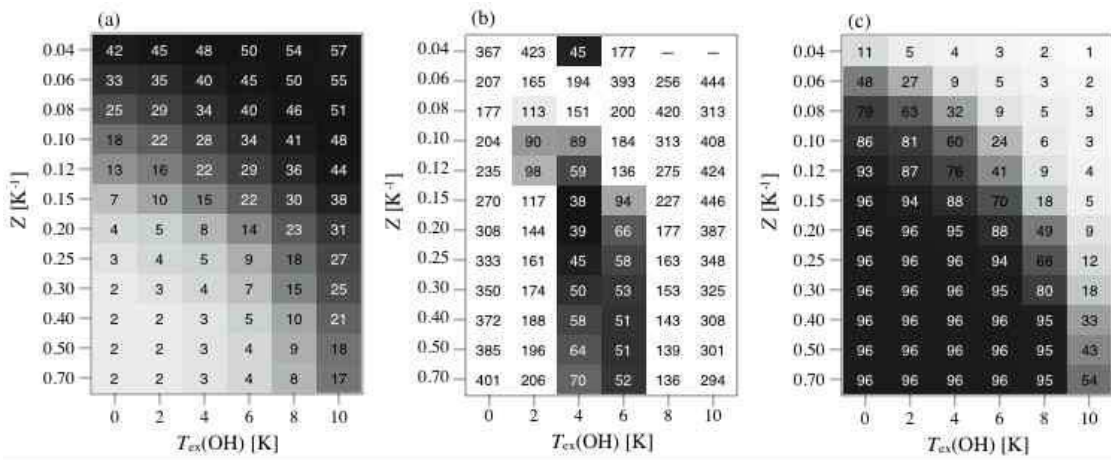


Figure 7. (a) Percentage of the CO emission within $|\ell| \leq 1^\circ$ which is located in the near side. The unit is per cent. (b) The standard deviation of the centres of CO emission in a cloud complex ($1^\circ 0 \leq \ell \leq 1^\circ 6$, $40 \leq v_{\text{LSR}} \leq 130 \text{ km s}^{-1}$) at $b = 0.0^\circ, \pm 0.2^\circ, \pm 0.4^\circ$ in parsecs. (c) Percentage of the CO emission in Clump 2 ($2^\circ 6 \leq \ell \leq 3^\circ 4$, $0.0^\circ \leq b \leq 0.4^\circ$, $30 \leq v_{\text{LSR}} \leq 200 \text{ km s}^{-1}$) which can be placed within the inner 3750 pc. The unit is per cent. Desirable parameter space is shadowed.

the lines of sight as noted later in § 3.1.3. The major axis of the condensation is inclined with respect to the line of sight ($x = 0$) by $\simeq 70^\circ$ so that the Galactic-eastern side is closer to us. This angle does not change significantly in the acceptable parameter space of $(Z, T_{\text{ex}}(\text{OH}))$. The condensation includes Sgr A ($\ell \simeq 0^\circ 0$), Sgr B ($\ell \simeq 0^\circ 6$), and Sgr C ($\ell \simeq -0^\circ 5$) molecular cloud complexes and the $1^\circ 3$ region. The resultant face-on distribution of radial velocity (Fig. 8b) clearly

shows that the gas motion in the condensation is strongly noncircular. The gas in the far-side has larger receding velocity, while the gas in the near-side is rather approaching. This velocity structure can be explained if the gas orbit is elongated along the major axis of the central condensation. It is a clear sign of a bar: a similar trend is often seen in both numerical simulations of gas kinematics in a barred potential and observations of barred galaxies (see, e.g., Athanassoula

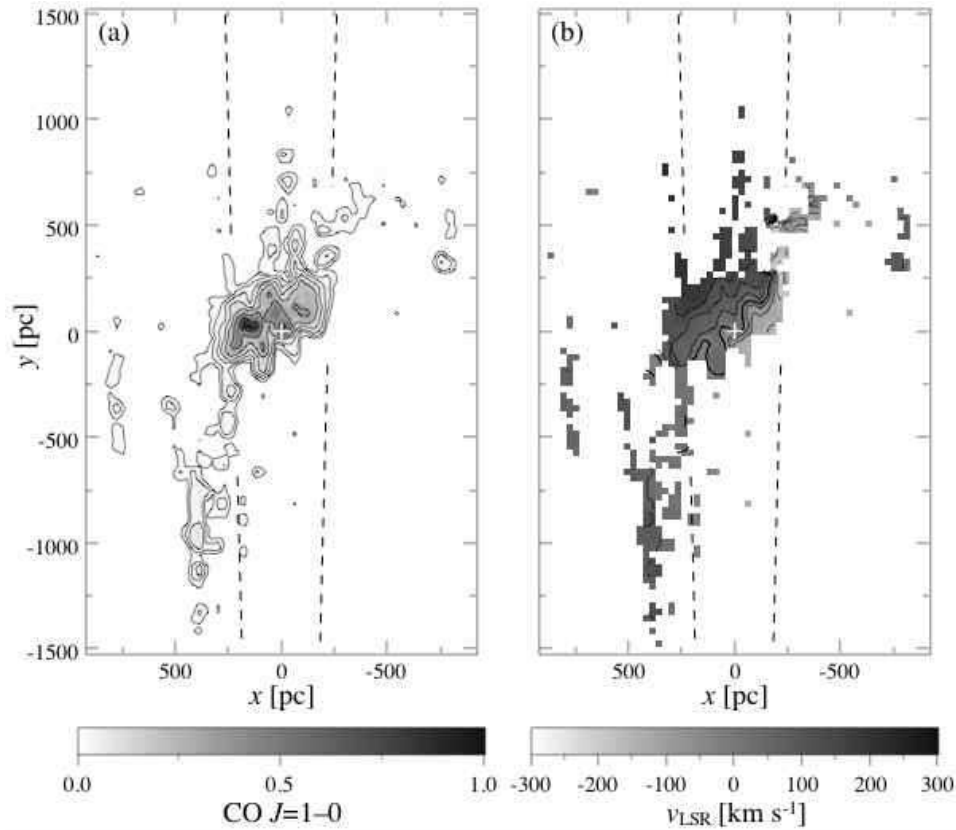


Figure 8. The resultant molecular face-on view of the Galactic centre at $b = 0^\circ 0$. The parameter set $(Z, T_{\text{ex}}(\text{OH})) = (0.15 \text{ K}^{-1}, 4 \text{ K})$ is used. Distribution of CO $J = 1 - 0$ emission (normalized by the peak value) is shown in (a). Contours are 0.01, 0.02, 0.04, 0.08, 0.16, 0.32, and 0.64 of the peak value. Corresponding radial velocity is shown in (b). Distribution of the velocity is shown in the region where the CO emission is more intense than 1 per cent of the peak. Contours are -200 to $+200 \text{ km s}^{-1}$ with a spacing of 50 km s^{-1} . Thick contour is $v_{\text{LSR}} = 0 \text{ [km s}^{-1}\text{]}$. The solar system is located at $(x, y) = (0, -8500)$. White crosses in both panels show the centre, $(x, y) = (0, 0)$. Dashed lines indicate $\ell = \pm 1.5^\circ$.

1992; Lindblad, Lindblad & Athanassoula 1996). This fact supports the arguments that the Milky Way is barred.

3.1.3 Bania's clump 2

The ridge, which lies at $(x, y) \simeq (400 \text{ pc}, -1000 \text{ pc})$, corresponds to the feature called Bania's Clump 2. Clump 2 has long been noticed because of its peculiar characteristics: widespread velocity structure and large latitudinal extent. Stark & Bania (1986) considered that Clump 2 can be understood as an end-on projection of a dust lane or an inner spiral arm. Fux (1999) argued that, however, a dust lane which associates with the Galactic-eastern side of the bar does not correspond to the Clump 2, but to the 'connecting arm' feature (Rougoor & Oort 1960) based on numerical simulation. Fux (1999) discussed Clump 2 and interpreted it as gas clouds which are crossing a dust lane shock.

In our face-on map, the ridge corresponding to Clump 2 resembles offset ridges (or dust lanes) often seen in barred spiral galaxies. Naively speaking, the entire structure, a central condensation and a possible offset ridge-like feature, is similar to those seen in central regions of barred galaxies (see, e.g., Kenney et al. 1992). It also mimics numerically simulated distributions of materials orbiting in a barred potential (see, e.g., Athanassoula 1992).

However, the elongation of the ridge along the line of sight might be artificial: the face-on maps obtained here inevitably involve positional errors along the lines of sight. The nominal error reduces around the centre since the gradient of continuum brightness (dT_{cont}/ds , namely, continuum emissivity j) becomes steeper; and vice versa. The 1σ deviations in T_{CO} and τ_{app} typically cause $\simeq 200 \text{ pc}$ error around Clump 2, while the error in the central condensation is a few tens of parsecs. A localized source of radio continuum emission embedded in the molecular cloud could also lead, in our model, to an apparently more widespread distribution of the cloud in the derived face-on map than the actual one.

Therefore our results cannot determine which of the interpretations [Stark & Bania (1986) and Fux (1999)] is relevant. Nevertheless, it is certain that Clump 2 lies in front of the centre, since the OH/CO ratio there is remarkably high.

3.1.4 'Expanding Molecular Ring' feature

The so-called EMR feature was considered as an expanding (and rotating) ring in the early works (Kaifu et al. 1972; Scoville 1972), as obvious from its name, based on its tilted oval ℓ - v appearance. Later, another interpretation that the apparent expansion results from elongated orbit of the gas was proposed. Binney et al. (1991) claimed that the ℓ - v lo-

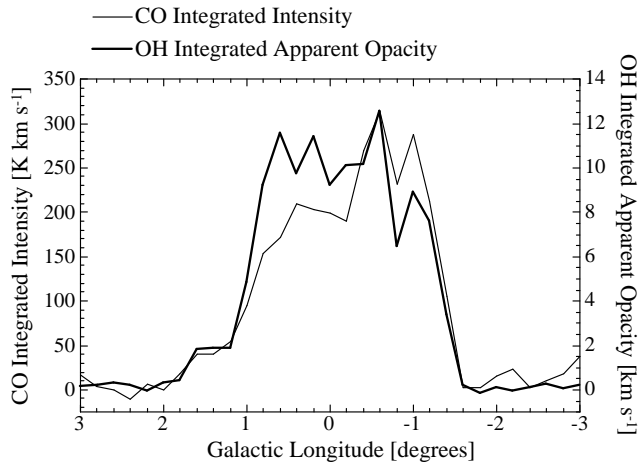


Figure 9. Longitudinal distribution of CO $J = 1 - 0$ integrated intensity (thin line) and OH integrated apparent opacity (thick line) for negative-velocity component of the EMR. The velocity range for the integration is $-300 \leq v_{\text{LSR}} [\text{km s}^{-1}] \leq -65 + 5\ell$ (ℓ is in degrees): approaching toward us faster than the hatched velocity ranges in Fig. 2.

cus of the EMR, a parallelogram rather than an ellipse, can be understood as a projection of the so-called x_1 orbit (Contopoulos & Mertzanides 1977) in a barred potential. As noted in the present (see § 2.1) and past (see, e.g., Kaifu et al. 1972) works, the negative-velocity component of the EMR lies in front of the centre, while the positive-velocity component is located behind the centre. Both interpretations, an expanding ring and an orbit in a barred potential, were constructed to match this geometry.

In the face-on map obtained in this work, the EMR (in particular negative-velocity component) is not clearly separated from the central condensation. We investigate the origin of the EMR, an energetic expansion or an orbital crowding, based on the OH/CO ratio. We would pay attention to the negative-velocity component of the EMR, which is prominently seen in ℓ - v diagrams at $b = 0^\circ 0, -0^\circ 2, -0^\circ 4$ (Fig. 5). Higher ratio is more extensively seen in the positive longitudes. For example, we present the longitudinal distribution of the CO emission and the OH absorption at $b = -0^\circ 2$ in Figure 9. The Figure shows the trend that the OH absorption is deeper in the positive longitudes compared with the CO emission. This suggests that the EMR, at least its negative-velocity component, is inclined so that the positive-longitude end is closer to us. This geometry agrees with the interpretation by Binney et al. (1991) rather than the axisymmetric ‘expanding ring’.

3.2 Physical conditions

Sawada et al. (2001) have investigated ℓ - v distribution of physical conditions of molecular gas in the Galactic centre using the CO intensity ratios ${}^{12}\text{CO } J = 2 - 1 / {}^{12}\text{CO } J = 1 - 0$ [$R_{2-1/1-0}({}^{12}\text{CO})$] and ${}^{13}\text{CO } J = 2 - 1 / {}^{12}\text{CO } J = 2 - 1$ [$R_{13/12}(J = 2 - 1)$]. In this subsection we discuss the face-on distribution of CO intensity ratios and physical conditions of the gas derived from the ratios.

In the face-on map derived in § 3.1 (Fig. 8), the Sgr B cloud complex at $(\ell, v_{\text{LSR}}) \simeq (0^\circ 6, 50 \text{ km s}^{-1})$ is mapped on

to $(x, y) \simeq (90 \text{ pc}, -100 \text{ pc})$. That is highly offset from the other part of the central condensation toward us, and the isovelocity contours are unnaturally curved around there. This is caused by the intense discrete continuum sources Sgr B1 and B2. Therefore we reassigned the cloud positions toward $\ell = 0^\circ 6$ by interpolating the velocity field from $\ell = 0^\circ 4$ and $0^\circ 8$: i.e., data at each velocity bin toward $\ell = 0^\circ 6$ are placed on to the position of the corresponding velocity in the interpolated velocity field. The resultant face-on maps of CO and corresponding radial velocity are presented in Figures 10a and 10b, respectively.

The velocity field in Fig. 10b can be used to convert an ℓ - v plot of any parameter (intensity of other lines, line intensity ratios, etc.) to a face-on view. We projected the ${}^{12}\text{CO } J = 2 - 1$ and ${}^{13}\text{CO } J = 2 - 1$ data (Sawada et al. 2001) at $b = 0^\circ 0$ on to the x - y plane. Figures 10c and 10d show the face-on distribution of intensity ratios $R_{2-1/1-0}({}^{12}\text{CO})$ and $R_{13/12}(J = 2 - 1)$, respectively. On one hand, $R_{2-1/1-0}({}^{12}\text{CO})$ is high (1.0–1.2) almost all over the central condensation. On the other hand, high $R_{13/12}(J = 2 - 1)$ (i.e., 0.10–0.15) is seen mainly within a radius of $\simeq 100 \text{ pc}$ around the centre.

Using one-zone large velocity gradient (LVG; see, e.g., Goldreich & Kwan 1974) analysis, Sawada et al. (2001) derived the physical conditions of the gas from these intensity ratios. Though the derived physical conditions depend on the assumed gas kinetic temperature T_k , the thermal pressure $p/k = n(\text{H}_2)T_k$ [$n(\text{H}_2)$ is the derived number density of molecular hydrogen] was found to be almost independent of the assumed T_k .

Figure 11a shows the distribution of pressure $n(\text{H}_2)T_k$ obtained in the same way. The highest pressure, $10^{4.9} - 10^{5.1} \text{ cm}^{-3} \text{ K}$, is seen within the central 100 pc. It is noteworthy that the highest pressure is found roughly symmetrically around the centre, whereas the molecular mass distribution is asymmetric in the way that the larger fraction of the CO emission comes from the positive longitude (see Fig. 10a). The central region corresponds to the ‘high pressure region’ in the ℓ - v diagram described in Sawada et al. (2001). Launhardt, Zylka & Mezger (2002) investigated the inner hundreds of parsecs of the Galaxy using *IRAS* and *COBE* data, and deduced that gas and dust within the galactocentric radius of 120 pc (referred to as ‘inner warm disk’ in their paper) are warmer than those at larger radii (‘outer cold torus’). The ‘high pressure region’ found in our analysis may correspond to the ‘inner warm disk’ in Launhardt et al. (2002). The $1^\circ 3$ region shows slightly lower pressure than the average of the central condensation; and the EMR has even lower pressure.

A schematic illustration of the major molecular features is shown in Figure 11b. Sofue (1995) identified a pair of arm-like features in the central condensation from the ${}^{13}\text{CO}$ data taken by Bally et al. (1987), though these ‘arms’ are not clearly separated in our face-on map. It may be due to insufficient spatial resolution of the present analysis and to deviation from the assumed smooth, axisymmetric continuum emissivity because of embedded discrete radio continuum sources. These arms and the high pressure region occupy a similar location in the ℓ - v diagram (Sawada et al. 2001). Oka et al. (1996) argued that formation of massive stars may have been taking place continuously or intermittently in this region for more than 10^8

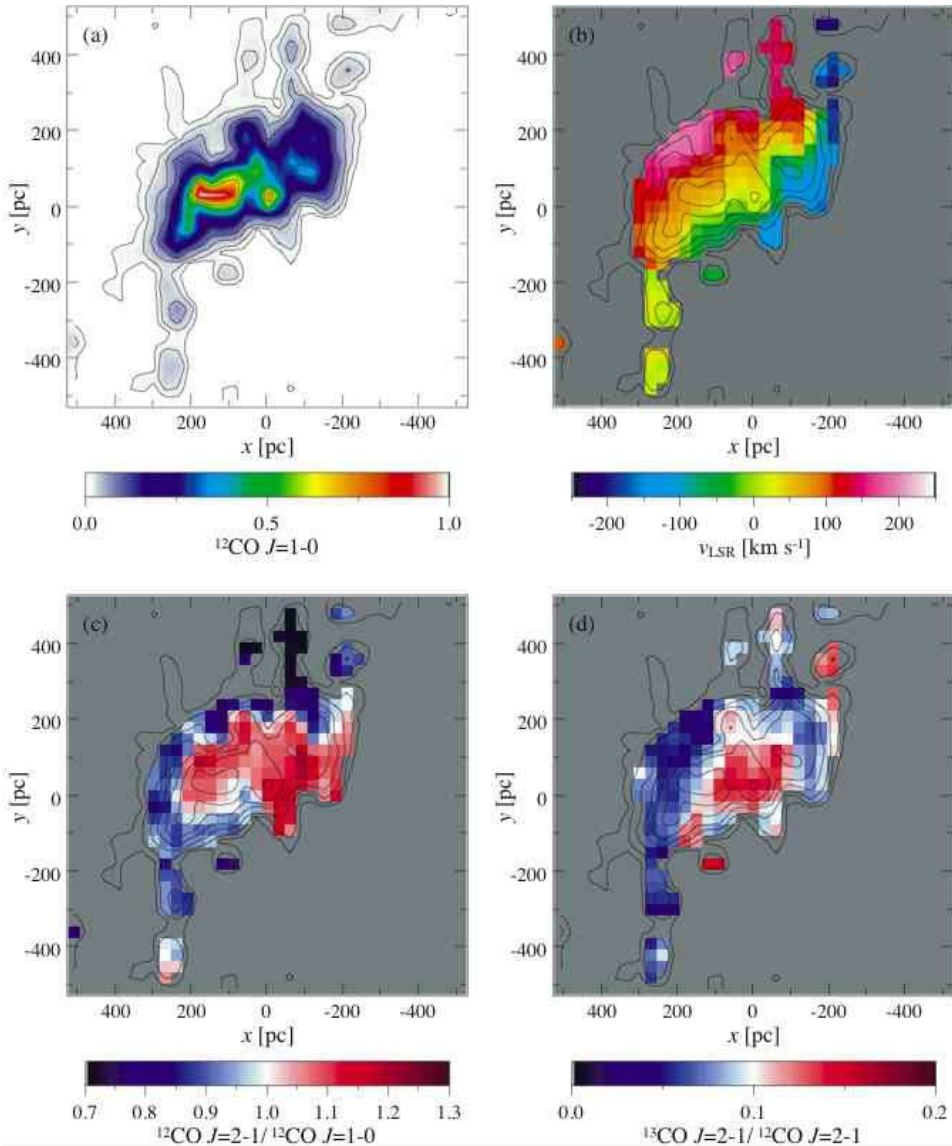


Figure 10. Face-on distribution (at $b = 0^\circ 0$) of (a) $^{12}\text{CO } J = 1 - 0$; (b) Radial velocity; (c) $^{12}\text{CO } J = 2 - 1 / ^{12}\text{CO } J = 1 - 0$ intensity ratio; and (d) $^{13}\text{CO } J = 2 - 1 / ^{12}\text{CO } J = 2 - 1$ intensity ratio. Values are shown in the region where the $^{12}\text{CO } J = 1 - 0$ emission is more intense than 2 per cent of the peak. Contours show the $^{12}\text{CO } J = 1 - 0$ distribution: levels are 0.01, 0.02, 0.04, 0.08, 0.16, 0.32, and 0.64 of the peak.

years based upon comparisons between their CO data and the ℓ - v distributions of H109 α recombination line emission (Pauls & Mezger 1975) and OH/IR stars (Lindqvist et al. 1991), and called it the ‘star-forming ring’. We consider that concentration of gas may occur to form high pressure (high density and/or high temperature) clouds in this region, from which stars form. Mizutani et al. (1994) observed the [C II] 158 μm line, which is considered to trace photodissociation regions, within $|\ell| \leq 0^\circ 7$ and found that the emission has peaks at Sgr B1 and Sgr C, in addition to Sgr A region. This might suggest that the star-forming activity is enhanced in the Sgr B and C regions. In the two-arm model by Sofue (1995), Sgr B and C are both located on the leads of these arms. In his analysis, ‘Arm I’ (which contains Sgr B) with lower (rather approaching) radial velocity is in the near side; ‘Arm II’ with Sgr C is in the far side. In our face-on map,

the far side of the central condensation shows larger receding velocity (see § 3.1). This geometry is consistent with that suggested by Sofue (1995), therefore Sgr B and C might be actually at the leads of these arms. The geometry that the sites of active star formation are located at the leads of inner arms may suggest a time lag between the arrival of the gas into the central orbit and the beginning of star formation as discussed by Kohno, Kawabe & Vila-Vilaró (1999) for NGC 6951.

The $1^\circ 3$ region lies at the Galactic-eastern end of the central condensation. Oka et al. (1998b) noted that the large velocity extents and the fluffy structure of the clouds and filaments in this region may be a sign that these clouds are formed by large-scale shocks. Hüttemeister et al. (1998) reported that SiO in this region is exceedingly abundant and its emission arises from hot, thin gas; which also indicates

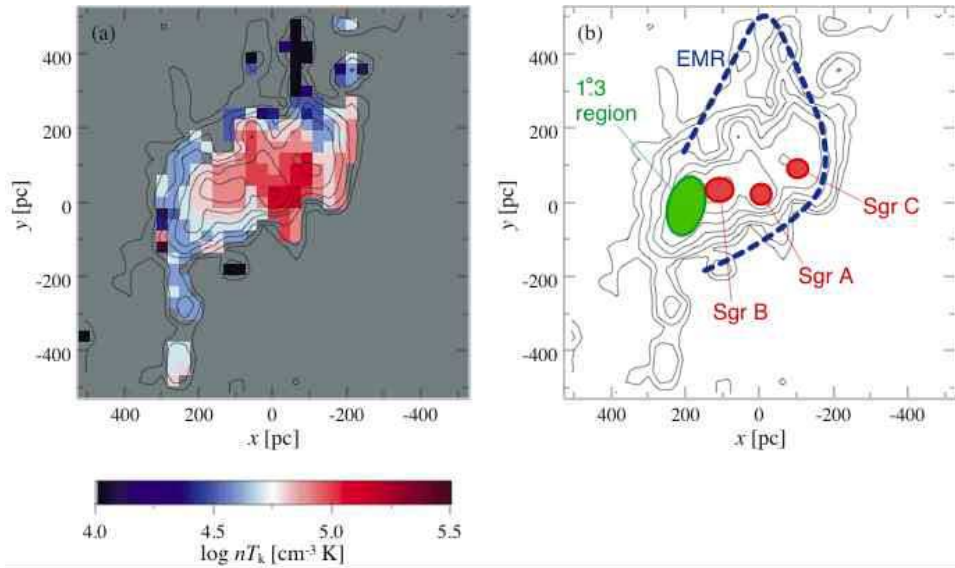


Figure 11. (a) Face-on distribution of gas thermal pressure derived from one-zone LVG analysis at $b = 0^{\circ}0$. Values are shown in the region where the ^{12}CO $J = 1 - 0$ emission is more intense than 2 per cent of the peak. (b) Schematic illustration of some molecular features. Contours in both panels are the same as those in Fig. 10.

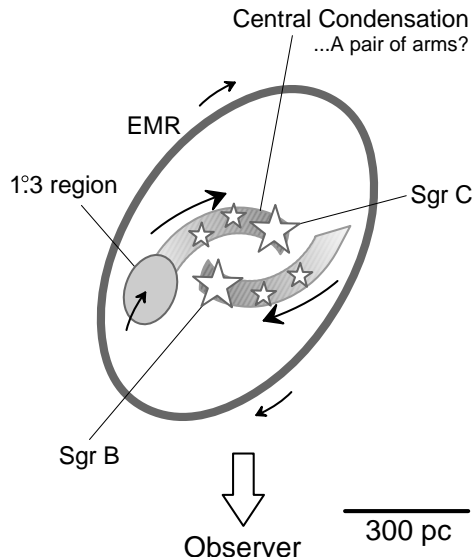


Figure 12. A picture of molecular gas in the Galactic centre region proposed on the basis of the results from this work. Linear scales are approximate.

the existence of shocks. From their arguments and its geometry, we suppose that the gas in the $1^{\circ}3$ region has recently arrived in the central region and collided with the central condensation. The extremely large scale height of this region compared with other parts of the central condensation supports our idea: the gas which has just fallen into the central gravitational field has not relaxed yet. The envelope of the $1^{\circ}3$ region toward the Galactic-east and smaller radial velocity is placed closer to us than the main body of the $1^{\circ}3$ region in the face-on map. This may support our idea that the $1^{\circ}3$ region has just bumped into the central condensation: the envelope may be a tail of the cloud that has not yet reached the condensation. Sakamoto, Baker & Scoville

(2000) suggested that ‘episodic fueling’ is occurring in NGC 5005: the $1^{\circ}3$ region might be a result of such kind of cloud infall. Our results are schematically summarized in Figure 12.

We have found that the major axis of the central condensation is inclined by an angle of $\simeq 70^{\circ}$ with respect to the line of sight. Therefore, the position angle between the major axes of the large-scale stellar bar and the central condensation is $\simeq 40^{\circ}\text{--}50^{\circ}$ (central condensation is leading the bar), if our viewing angle of the bar is $\simeq 20^{\circ}\text{--}30^{\circ}$ (see Morris & Serabyn 1996; Gerhard 1999; Deguchi et al. 2002, and references therein). In some barred galaxies, there are central molecular gas concentrations (‘twin peaks’, Kenney et al. 1992). In a face-on projection of high resolution images, some of these concentrations tend to consist of a pair of arms and their major axes are inclined with respect to the bar major axes by moderate angles: such as IC 342 by Ishizuki et al. (1990), M101 etc. by Kenney et al. (1992), NGC 1530 by Reynaud & Downes (1999), NGC 6951 by Kohno et al. (1999), NGC 5383 by Sheth et al. (2000), and NGC 4303 by Schinnerer et al. (2002). They are similar to our face-on view of the Galactic centre. Hydrodynamical simulations of the barred galaxies also produce similar gas distributions: e.g., simulations for NGC 1365 made by Lindblad et al. (1996) produce a central condensation which is inclined from the bar axis with a similar angle as that we have obtained, $40^{\circ}\text{--}50^{\circ}$. Binney et al. (1991) interpreted the longitude-velocity feature that corresponds to the central condensation as a projection of gaseous materials in x_2 orbits. However the x_2 orbits are aligned perpendicular to the potential (Fig. 3 in Binney et al. 1991). As a result, the sense of inclination with respect to the line of sight are opposite between our and their interpretation. This difference may be due to the fact that the x_2 orbits perpendicular to the bar are stellar (collisionless) orbits. Wada (1994) showed from his damped-orbit model that gaseous orbits do not align with respect to the bar but their major axes gradually

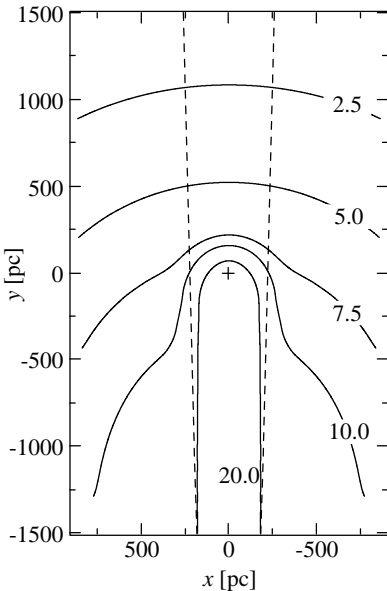


Figure 13. Contours of integrated continuum emissivity $\int_{-\infty}^{s_0} j(r)ds$ (see Eq. (1)) at $b = 0^{\circ}0$ based upon the 3 Gaussians model. Contour levels are 2.5, 5.0, 7.5, 10.0, and 20.0 K in units of brightness temperature. A molecular cloud located on this plane should be seen in emission if $T_{\text{ex}}(\text{OH})$ is higher than the integrated continuum emissivity shown by the contours. Coordinates are the same as Fig. 8. The centre $(x, y) = (0, 0)$ is shown by a cross. Dashed lines indicate $\ell = \pm 1^{\circ}5$.

changes with the Galactocentric radius. He showed that the orbits at the Inner Lindblad Resonances lead the bar by 45° : the trend agrees with the gas distribution we have obtained.

3.3 Validity of parameters

3.3.1 Beam filling factor

We have assumed that f , the beam filling factor of the OH absorbing gas, is equal to unity. From Eq. (1), we can show $f > \tau_{\text{app}}$: f gets the lowest if the cloud is located in the solar neighborhood and has infinite opacity. For some lines of sight, the apparent opacity τ_{app} , which is the lower limit of f , is rather large: 0.64 toward Sgr B2; 0.35 toward the $1^{\circ}3$ region and Clump 2. This fact supports that the beam filling factor is large and can be reasonably replaced with unity.

Sawada et al. (2001) estimated the beam filling factor of CO $J = 1 - 0$ emission to be 0.4–0.7 based upon the LVG analyses and high resolution CO data taken by Oka et al. (1998b). Moreover, since it is expected that the OH absorption arises also from less dense cloud envelope compared with the CO emission, the beam filling factor of OH absorbing gas is at least similar and can be even larger. This again suggests that f is nearly unity.

3.3.2 Excitation temperature

We have assumed that the excitation temperature of OH, $T_{\text{ex}}(\text{OH})$, is uniformly 4 K above the CMB. It is reported that $T_{\text{ex}}(\text{OH})$ typically ranges in 5–10 K (Elitzur 1992). Our value, 4 K + T_{CMB} , is close to this.

Figure 13 shows contours of integrated continuum emissivity along lines of sight, $\int_{-\infty}^{s_0} j(r)ds$ in Eq. (1), at $b = 0^{\circ}0$. It is expected that the gas behind the contour which is equal to $T_{\text{ex}}(\text{OH})$ is seen in emission, while the gas in front of the contour is seen in absorption. However, no significant OH emission is observed in this region. Thus, if $T_{\text{ex}}(\text{OH}) \gtrsim 6$ [K], the face-on gas distribution is almost restricted to near side of the Galactic centre, $y < 0$. We consider it is unrealistic. On the other hand, Boyce & Cohen (1994) noted that the OH absorption was only detected at positions where the continuum temperature exceeded 5 K of antenna temperature (7.5 K of brightness temperature). Lower limit of excitation temperature of OH is provided from this fact: $T_{\text{ex}}(\text{OH})$ is higher than the integrated continuum emissivity if the OH lines are not seen as absorption. For a cloud in the Galactic centre region, integrated continuum emissivity at the position of the cloud is typically a half of the observed brightness temperature. Thus $T_{\text{ex}}(\text{OH})$ should not be far below (7.5/2) K.

Again using Eq. (1), we can show that the upper limit of $T_{\text{ex}}(\text{OH})$ is described as $(1 - \tau_{\text{app}}) \int_{-\infty}^{s_0} j(r)ds$: $T_{\text{ex}}(\text{OH})$ gets the highest if the cloud is located in the solar neighborhood. Toward Clump 2, this value goes down to 7 K, which gives a similar constraint to $T_{\text{ex}}(\text{OH}) \lesssim 6$ [K] derived above. On the other hand, our trials have shown that almost all clouds are placed on the far side of the Galactic centre ($y > 0$) at high Galactic latitudes if $T_{\text{ex}}(\text{OH})$ is lower ($\lesssim 3$ [K]).

In conclusion, 4 K is a proper estimate of the excitation temperature.

3.3.3 The 'Z' factor

We have derived Z , the factor to convert T_{CO} into τ_{OH} , in § 2.2 empirically. Here we attempt an independent estimate of Z .

There are three previously-known relations. (1) It is considered that the column density of molecular hydrogen $N(\text{H}_2)$ is proportional to the CO $J = 1 - 0$ integrated intensity. The conversion factor (the so-called X -factor) is measured to be about $2 \times 10^{20} [\text{cm}^{-2} (\text{K km s}^{-1})^{-1}]$ for molecular clouds in the Galactic disc (see, e.g., Dame, Hartmann & Thaddeus 2001). For the Galactic centre clouds, however, it is reported that the X -factor is smaller than that for the Galactic disc: i.e., $X = \text{several} \times 10^{19}$ (see, e.g., Oka et al. 1998a). (2) Relative abundance of OH to molecular hydrogen, $[\text{OH}]/[\text{H}_2]$, is typically several $\times 10^{-7}$ (see, e.g., Herbst & Leung 1989). (3) The OH column density is derived from the OH 1667 MHz opacity τ as $N(\text{OH}) = 2 \times 10^{14} T_{\text{ex}} \int \tau dv$.

Using these relations, the Z factor is written as

$$Z [\text{K}^{-1}] = \frac{[\text{OH}]/[\text{H}_2]}{2 \times 10^{14}} \frac{X [\text{cm}^{-2} (\text{K km s}^{-1})^{-1}]}{T_{\text{ex}} [\text{K}]} \quad (7)$$

$$= 5 \times 10^{-3} \frac{[\text{OH}]/[\text{H}_2]}{10^{-7}} \frac{X}{10^{20} \text{cm}^{-2} (\text{K km s}^{-1})^{-1}} \frac{10 \text{K}}{T_{\text{ex}}} \quad (8)$$

This value becomes several $\times 10^{-2}$, which is several times smaller than that we have adopted. However $Z \simeq \text{several} \times 10^{-2}$ does not seem to be realistic, because such a small Z cannot reproduce the observed absorption depth for a significant fraction of the clouds. This discrepancy can be solved if we consider larger X (several $\times 10^{20}$) or higher OH abun-

dance (several $\times 10^{-6}$). On one hand, the large X -factor is unrealistic because the small X -factor in the Galactic centre region is consistently suggested in various ways (see, e.g., Blitz et al. 1985; Cox & Laureijs 1989; Sodroski et al. 1995; Oka et al. 1998a). On the other hand, it is reported that the OH abundance is enhanced behind interstellar shocks (see, e.g., Wardle 1999). In a high resolution CO map of the Galactic centre, innumerable shells/arcs are seen (Oka et al. 1998b, 2001a,b). If the shells/arcs are formed by a number of explosive phenomena such as supernova, the Galactic centre is filled with shocks. In such condition, the OH abundance may be higher than that in usual condition. High ionization rate caused by X-ray also enhances the OH abundance (Lepp & Dalgarno 1996).

3.3.4 One-to-one correspondence between position and velocity

In § 2.2, we have assumed that a value in the radial velocity corresponds to a single position at a given line of sight. Of course this assumption is nominally wrong: there are two (or more) points in a line of sight with a given radial velocity. Thus, if the Galactic centre region is almost filled with molecular gas, the assumption becomes fairly wrong. Molecular gas distribution is, however, rather localized. In fact, our (Fig. 2) and higher-resolution (see, e.g., Oka et al. 1998b) molecular line data show that velocity overlapping between major features (Sofue's arms, EMR, etc.) occurs in very restricted regions. Therefore the assumption might not introduce serious errors into the resultant face-on maps.

Even if overlapping of clouds is occurring, the results do not change very much: let we assume that two individual clouds (positions s_1 and s_2 ; $s_1 < s_2$) with the same velocity is seen as a single cloud. Position of this 'cloud' is derived as s_0 in our method. Using Eq. (1), we can show $s_1 < s_0 < s_2$ if the H₂ column density can be fully traced by T_{CO} . Thus the overall CO distribution derived is not heavily affected in this situation.

4 CONCLUSIONS

We have developed a method to derive positions of molecular clouds along the lines of sight. The method is completely independent of any kinematic model and based on observable data alone; the CO emission line, the OH absorption line, and 18 cm continuum distribution. It is applied to the central region of the Milky Way to obtain a molecular face-on map. The obtained spatial and kinematical structure of molecular gas shows the following characteristics.

- The CO distribution mainly consists of a central condensation and a ridge.
- The central condensation is elongated and its major axis is inclined with respect to the line of sight by $\simeq 70^\circ$ so that the Galactic-eastern end is closer to us. The gas within it shows highly noncircular motion: the gas in the far side is receding whereas the gas in the near side is approaching. This noncircularity of the gas motion is most likely induced by a barred potential.
- The ridge, corresponding the Bania's Clump 2, lies closer to us than the central condensation by $\simeq 1$ kpc. This

feature apparently mimics offset ridges often seen in barred galaxies, although its stretch along our line of sight might be artificial.

- The so-called 'Expanding Molecular Ring' feature does not appear as a coherent structure on the resultant face-on map. However its negative-velocity side, which lies in the near side of the Galactic centre, is inclined so that the Galactic-eastern side is closer to us. This is consistent with the arguments by Binney et al. (1991), that the EMR is a projection of x_1 orbit in a barred potential, rather than the original picture of a ring that is expanding and rotating.

These results give a new evidence for the existence of a bar in the Milky Way Galaxy based on direct distance derivation independent of kinematic models. A face-on map of thermal pressure derived from comparison of three CO transition lines and an LVG analysis is also presented. The pressure is distinctly higher (i.e., $\gtrsim 10^5 \text{ cm}^{-3} \text{ K}$) within the Galactocentric radius of 100 pc, compared with the outer region. This high pressure region coexists with 'Galactic centre arms' (Sofue 1995) and 'star-forming ring' (Oka et al. 1996). Concentration of clouds would be occurring due to some kind of gas orbit crowding.

ACKNOWLEDGMENTS

We acknowledge Leonardo Bronfman for providing us the CO $J = 1 - 0$ data in a computer readable form. This work was supported by a Grant-in-Aid for Scientific Research of the Ministry of Education, Culture, Sports, Science, and Technology 08404009 and 10147202.

REFERENCES

- Athanassoula E., 1992, MNRAS, 259, 345
- Bally J., Stark A. A., Wilson R. W., Henkel C., 1987, ApJS, 65, 13
- Bally J., Stark A. A., Wilson R. W., Henkel C., 1988, ApJ, 324, 223
- Bania T. M., 1977, ApJ, 216, 381
- Binney J., Gerhard O. E., Stark A. A., Bally J., Uchida K. I., 1991, MNRAS, 252, 210
- Bitran M., Alvarez H., Bronfman L., May J., Thaddeus P., 1997, A&AS, 125, 99
- Blitz L., Bloemen J. B. G. M., Hermsen W., Bania T. M., 1985, A&A, 143, 267
- Boyce P., Cohen R. J., 1994, A&AS, 107, 563
- Cohen R. J., Dent W. R. F., 1983, in Burton W. B., Israel, F. P., eds., Surveys of the Southern Galaxy. Reidel, Dordrecht, p. 159
- Cohen R. J., Few R. W., 1976, MNRAS, 176, 495
- Contopoulos G., Mertzanides C., 1977, A&A, 61, 477
- Cox P., Laureijs R., 1989, in Morris M., ed., Proc. IAU Symp. 136, The Center of the Galaxy. Kluwer, Dordrecht, p. 121
- Crosthwaite L. P., Turner J. L., Ho T. P. T., 2000, AJ, 119, 1720
- Dame T. M., Hartmann D., Thaddeus P., 2001, ApJ, 547, 792
- Deguchi S., Fujii T., Nakashima J., Wood P. R., 2002, PASJ, 54, 719

Elitzur M., 1992, Astronomical Masers. Kluwer, Dordrecht

Fux R., 1999, *A&A*, 345, 787

Gerhard O. E., 1999, in Merritt D., Valluri M., Sellwood J., eds., *ASP Conf. Ser. Vol. 182, Galaxy Dynamics*. Astron. Soc. Pac., San Francisco, p. 307

Goldreich P., Kwan J., 1974, *ApJ*, 189, 441

Herbst E., Leung C. M., 1989, *ApJS*, 69, 271

Hummel E., van der Hulst J. M., Keel W. C., 1987, *A&A*, 172, 32

Hüttemeister S., Dahmen G., Mauersberger R., Henkel C., Wilson T. L., Martín-Pintado J., 1998, *A&A*, 334, 646

Ishizuki S., Kawabe R., Ishiguro M., Okumura S. K., Morita K.-I., Chikada Y., Kasuga T., 1990, *Nat*, 344, 224

Kaifu N., Kato T., Iguchi T., 1972, *Nature Phys. Sci.*, 238, 105

Kenney J. D. P., Wilson C. D., Scoville N. Z., Devereux N. A., Young J. S., 1992, *ApJ*, 395, L79

Kohno K., Kawabe R., Vila-Vilaró B., 1999, *ApJ*, 511, 157

Launhardt R., Zylka R., Mezger P. G., 2002, *A&A*, 384, 112

Lepp S., Dalgarno A., 1996, *A&A*, 306, L21

Lindblad P. A. B., Lindblad P. O., Athanassoula E., 1996, *A&A*, 313, 65

Lindqvist M., Winnberg A., Habing H. J., Matthews H. E., 1991, *A&AS*, 92, 43

Liszt H. S., Burton W. B., 1980, *ApJ*, 236, 779

Mizutani K. et al., 1994, *ApJS*, 91, 613

Morris M., Serabyn E., 1996, *ARA&A*, 34, 645

Nakanishi H., Sofue Y., 2003, *PASJ*, 55, 191

Oka T., Hasegawa T., Handa T., Hayashi M., Sakamoto S., 1996, *ApJ*, 460, 334

Oka T., Hasegawa T., Hayashi M., Handa T., Sakamoto S., 1998a, *ApJ*, 493, 730

Oka T., Hasegawa T., Sato F., Tsuboi M., Miyazaki A., 1998b, *ApJS*, 118, 455

Oka T., Hasegawa T., Sato F., Tsuboi M., Miyazaki A., 2001a, *PASJ*, 53, 779

Oka T., Hasegawa T., Sato F., Tsuboi M., Miyazaki A., 2001b, *PASJ*, 53, 787

Ondrechen M. P., 1985, *AJ*, 90, 1474

Ondrechen M. P., van der Hulst J. M., 1983, *ApJ*, 269, L47

Pauls T., Mezger P. G., 1975, *A&A*, 44, 259

Reynaud D., Downes D., 1999, *A&A*, 347, 37

Rougoor G. W., Oort J. H., 1960, *Proc. Nat. Acad. Sci.*, 46, 1

Sakamoto K., Baker A. J., Scoville N. Z., 2000, *ApJ*, 533, 149

Sandqvist Aa., Jörsäter S., Lindblad P. O., 1995, *A&A*, 295, 585

Sawada T. et al., 2001, *ApJS*, 136, 189

Schinnerer E., Maciejewski W., Scoville N., Moustakas L. A., 2002, *ApJ*, 575, 826

Scoville N. Z., 1972, *ApJ*, 175, L127

Sheth K., Regan M. W., Vogel S. N., Teuben P. J., 2000, *ApJ*, 532, 221

Sodroski T. J. et al., 1995, *ApJ*, 452, 262

Sofue Y., 1995, *PASJ*, 47, 527

Stark A. A., Bania T. M., 1986, *ApJ*, 306, L17

Wada K., 1994, *PASJ*, 46, 165

Wardle M., 1999, *ApJ*, 525, L101